J BONE ONCOL 44 (2024) 100517

Contents lists available at ScienceDirect

Journal of Bone Oncology

journal homepage: www.elsevier.com/locate/jbo

Research Paper

Essential genes analysis reveals small ribosomal subunit protein eS28 may be a prognostic factor and potential vulnerability in osteosarcoma

Chao Liang [a,b,1], Juan Zhou [c,1], Yongjie Wang [d,1], Yin Sun [b], Jin Zhou [b], Lan Shao [b], Zhichang Zhang [b], Wangjun Yan [a,*], Zhiyan Liu [c,*], Yang Dong [b,*]

[a] Department of Musculoskeletal Oncology, Fudan University Shanghai Cancer Center, Shanghai Medical College, Fudan University, Shanghai, 200032, PR China
[b] Department of Orthopedics, Shanghai Sixth People's Hospital Affiliated to Shanghai Jiao Tong University School of Medicine, Shanghai 200233, PR China
[c] Department of Pathology, Shanghai Sixth People's Hospital Affiliated to Shanghai Jiao Tong University School of Medicine, Shanghai 200233, PR China
[d] Department of Orthopedics, Shanghai Tenth People's Hospital, Tongji University School of Medicine, Shanghai, 200072, PR China

HIGHLIGHTS

- Essential Genes analysis reveals *Rps28* is an essential gene for osteosarcoma cell lines.
- Small ribosomal subunit protein eS28 may be a Prognostic Factor and Potential Therapeutic Target in Osteosarcoma.
- Silencing Rps28 affected the MAPK signaling pathway in osteosarcoma.

ARTICLE INFO

Keywords:
Osteosarcoma
CRISPR/Cas9 library
Ribosome biogenesis
RPS28
eS28
MAPK signal pathways

ABSTRACT

Background: Osteosarcoma, the most common primary malignant bone tumor, is currently treated with surgery combined with chemotherapy, but the limited availability of targeted drugs contributes to a poor prognosis. Identifying effective therapeutic targets is crucial for improving the prognosis of osteosarcoma patients.
Methods: We screened the DepMap database to identify essential genes as potential therapeutic targets for osteosarcoma. Gene Set Enrichment Analysis (GSEA) was employed to elucidate the biological roles of these essential genes. Promising candidates were filtered through univariate and multivariate Cox analyses, as well as Kaplan-Meier survival analyses using the GSE21257-OSA and TARGET-OSA datasets. The functional role of the target gene was assessed through cell experiments. Additionally, an in situ nude mice model was established to observe the gene's function, and RNA sequencing was utilized to explore the underlying molecular mechanism.
Results: A total of 934 essential genes were identified based on their effects (Chronos) using the DepMap database. These genes were primarily enriched in the ribosome pathway according to GSEA analysis. Among them, 195 genes were associated with the ribosome pathway. *Rps28*, *Rps7*, and *Rps25* were validated as promising candidates following univariate and multivariate Cox analyses of the TARGET-OSA and GSE21257-OSA datasets. Kaplan-Meier survival analyses indicated *Rps28* represented an especially promising target, with high expression correlating with poor prognosis. Knockdown of small ribosomal subunit protein eS28, the protein of *Rps28*, inhibited proliferation, migration, and invasion in both in *vitro* and in *vivo* experiments. Silencing *RPS28* affected the MAPK signaling pathway in osteosarcoma.
Conclusion: In summary, *Rps28* has been identified as an essential gene for osteosarcoma cell survival and eS28 may serve as a potential vulnerability in osteosarcoma.

1. Introduction

Osteosarcoma (OSA), the most prevalent primary malignant solid tumor affecting bone, primarily affects adolescents, with a second peak in incidence among adults over the age of 65 [1]. The standard treatment for OSA, consisting of neoadjuvant chemotherapy and surgical

* Corresponding authors.
E-mail addresses: yanwj@fudan.edu.cn (W. Yan), zhiyanliu@shsmu.edu.cn (Z. Liu), dongyang6405@163.com (Y. Dong).
[1] These authors contributed equally to this work.

https://doi.org/10.1016/j.jbo.2023.100517
Received 28 September 2023; Received in revised form 26 November 2023; Accepted 13 December 2023
Available online 15 December 2023

resection of the primary tumor followed by adjuvant chemotherapy, was established in the 1980s and has gradually evolved to achieve long-term survival rates exceeding 70 % in patients with localized disease [2,3]. However, the limited progress in drug development over the past four decades has hindered advancements in OSA patient survival [4]. Consequently, it is imperative to identify effective therapeutic targets for individuals with OSA.

CRISPR screens for loss of function, including both genome-wide and large sub-genome screens, have become increasingly essential for studying gene function in both normal and disease conditions [5,6]. Researchers infect cells with a library of single-guide RNAs (sgRNAs) targeting specific interest genes. The Broad and Sanger Institutes conducted genome-wide CRISPR-KO screenings, using hundreds of cancer cell lines to comprehensively understand gene dependencies in cancer cells. Their collaborative effort resulted in the development of the DepMap database, which houses the screening data, aiming to facilitate data sharing and knowledge exchange in cancer research [7]. CRISPR libraries, through positive selection, enable the identification of cells that survive under specific conditions, such as drug treatment, aiding in the elucidation of drug resistance mechanisms. On the other hand, negative selection efficiently detects nonviable or slowly growing cells, enabling the identification of genes essential for cell survival. Such genes hold promise as potential targets for molecularly targeted drugs [8,9]. Moreover, the Chronos algorithm is an advanced model that incorporates an explicit model of cell population behavior in CRISPR screens. This enhancement improves the inference of gene fitness effects beyond the capabilities of current state-of-the-art methods [10].

In this study, our main goal was to identify crucial genes essential for the survival of osteosarcoma cells. To achieve this, we employed various methods, including screening the DepMap database, conducting Gene Set Enrichment Analysis (GSEA), univariate and multivariate COX regression analysis, and Kaplan-Meier methods. The validity of our findings was confirmed through both in *vitro* and in *vivo* experiments. Additionally, we performed RNA sequencing to explore the underlying molecular mechanism. By studying essential genes, our research aimed to contribute to the identification and investigation of novel therapeutic targets, thus having significant implications for future treatment strategies.

2. Methods

2.1. DepMap analysis

DepMap (https://depmap.org/portal/) is an accessible website based on large-scale multi-omics screening projects based on CRISPR-Cas9 and RNAi [11]. The Chronos algorithm was used for the determination of dependency scores. Chronos is an algorithm that leverages an explicit model of cell population behavior in CRISPR screens to enhance the inference of gene fitness effects beyond the current state of the art. A lower Chronos score indicates a higher likelihood that the gene of interest is essential in given cell lines. Negative scores represented these genes were essential in the proliferation of OS cells [10].

2.2. GSEA analysis

In this study, GSEA analysis for essential genes was used by "fgsea" packages. Genome expression profiles in the si-RPS28 and si-control groups were analyzed using GSEA software and enrichment score (ES) was calculated.

2.3. Immunohistochemistry

OSA tissues and paratumor soft tissues were obtained from five OSA patients who underwent limb-sparing or amputation surgery from January to June 2021. This study followed standard guidelines and was approved by the Ethics Committee of Shanghai Jiao Tong University Affiliated Sixth People's Hospital (Approval No: 2021-275), PR China. Written informed consent was obtained from all participants, whose demographic information and clinicopathological characteristics were displayed in Table 1. OSA tissues were fixed in 4 % paraformaldehyde. All tissues were dehydrated and embedded in paraffin. Subsequently, 4 μm thick tissue sections were stained with primary antibodies against RPS28 (Sigma-Aldrich Cat# HPA047132, dilution 1:100, Saint Louis, State of Missouri, USA) and a horseradish peroxidase-conjugated IgG (Servicebio, Wuhan, China). The staining results were shown by diaminobenzidine (DAB), scanned using the NDP Nano Zoomer S210 (Hamamatsu, ShizuokaPref, Japan), and analyzed with the NDP view 2.0 software. A semiquantitative method according to the staining intensity and the positive rate was used to score the staining. The intensity was defined as follows: 0, negative; 1, weak; 2, moderate; and 3, strong. The positive rate was defined as follows: 0, < 1 %; 1, 1–25 %; 2, 26–50 %; 3, 51–75 %; and 4, 75–100 %. IHC score > 6 and ≤ 6 were considered as high and low expression, respectively.

2.4. Cell line and cell culture

All of the human OSA cell lines were purchased from the Chinese Academy of Sciences (Shanghai, China) and cultured in Dulbecco's modified Eagle's medium (DMEM) (Hyclone, Tauranga, New Zealand) with 10 % fetal bovine serum (FBS) (Gibco, NY, USA), as well as penicillin (100 U/ml) and streptomycin (100 μg/ml) (Invitrogen, CA, USA) at 37 °C in a humidified 5 % CO_2 atmosphere.

2.5. RNA extraction and quantitative real-time-PCR

Total RNA was isolated using trizol reagent (Life Technologies, CA, USA), then used to synthesize complementary DNA using the iScript™ cDNA Synthesis Kit (Bio-Rad, CA, USA). Subsequently, quantitative real-time PCR was conducted using SYBR pre-mix Ex Taq (Takara, Liaoning, China) and ABI 7500 Sequence Detection System (Thermo Fisher Scientific, MA, USA). All procedures were performed according to the manufacturer's protocols. Relative expression was calculated using the $2^{-\Delta\Delta Cq}$ method with GAPDH as the endogenous reference gene. The sequences of primers used are listed as follows: GAPDH, forward, 5′-GGAGCGAGATCCCTCCAAAAT-3′ and reverse, 5′-GGCTGTTGTCATACTTCTCATGG-3′; RPS28, forward, 5′-GACACGAGCCGATCCATCATC-3′ and reverse, 5′-TGACTCCAAAAGGGTGAGCAC-3′.

2.6. RNA interference and construction of shRNA vector

RPS28 siRNA duplexes and corresponding si-control were purchased from Ri-boBio (Guangzhou, China). The sequences targeting RSP28 were as follows: si-RPS28-1, 5′-CCATCATCCGCAATGTAAA-3′; si-RPS28-2, 5′-GCTCACCCTTTTGGAGTCA-3′; si-RPS28-3, 5′-TGCGCGTGGAATTCATGGA-3′. The control si-RNA (siN0000001-1-5) was provided by Ribobio. According to the manufacturer's protocol, transient transfections were performed with Lipofectamine 3000 (Invitrogen, CA, USA).

VIRUS-Free™ carriers were constructed as follows: pPB[shRNA]-Hygro-U6 > vectors containing specific shRNAs, including hRPS28shRNA#1(NO.TSC239-1), shRNA#2(NO.TSC239-2), and scramble shRNA#1 (NO.TSC239-3) were designed and constructed according to the nucleotide sequence in above-mentioned si-RPS28-1 and si-RPS28-3, respectively. The construction involved designing and assembling these vectors. Large-scale extraction of transfected low endotoxin nucleic acid was conducted. Electrical conversion was performed by Neon ™ Transfector (Cat # MPK5000). After 48 h of cell culture, the target cells after electroporation were screened using the 800 μg/mL hygromycin B. After the end of the drug screening, drug-containing culture medium was removed and replaced with fresh culture medium. Then, the cells were allowed to recover for 48 h. Subsequently, western blotting was performed to test the efficiency of RPS28

Table 1
Demographic information and clinicopathological characteristics of the patients in our cohort.

Ethnicity	Gender	Age	Tumor side	Tumor site	Tumor region	Eenneking stage	Surgery	Tumor necrosis rate	Pathological diagnosis
Han	Male	38	Right	Femur	Distal	III	Limb-sparing	85 %	Classical OSA
Han	Male	20	Right	Femur	Distal	III	Amputation	5 %	Classical OSA
Han	Male	42	Left	Femur	Proximal	IIB	Limb-sparing	30 %	Classical OSA
Han	Female	10	Right	Tibia	Proximal	IIB	Limb-sparing	15 %	Classical OSA
Han	Female	9	Left	Tibia	Proximal	IIB	Limb-sparing	66 %	Classical OSA

knock-down.

2.7. Western blotting analysis

Protein was extracted from treated MG63 and 143B using RIPA lysis buffer (Biosharp, China), whose concentration was assessed using the Protein Quantification Kit (Thermo Fisher Scientific, USA). Cell homogenates containing equal amounts of protein were separated on 10 % and 12 % SDS-PAGE and then transferred on polyvinylidene difluoride membranes (Merck, Germany), which were blocked with 5 % skimmed milk for 1 h at room temperature. After being incubated with primary antibody (1:1000) overnight at 4 °C, the membranes were washed twice with TBST and incubated with horseradish peroxidase (HRP)-linked secondary antibodies (1:5000) at room temperature for 1 h. ECL Kit (Sharebio, Shanghai, China) was used to visualize the blots. The primary antibodies used were p44/42 MAPK (cat. No.4695T, CST), c-myc (cat. No. 5605T), phospho-MAPK Family Antibody Sampler Kit (cat. No.9910T, CST), RPS28 Rabbit pAb (A17937) (Abclonal, Wuhan, China), and β-Tubulin (cat. No.2148S, CST). The secondary antibody used was HRP Goat Anti-Rabbit IgG (cat. No.7074P2, CST). Protein bands were visualized using an enhanced chemiluminescence (ECL) kit. Fiji Image J Software was used to measure the grayscale analysis.

2.8. Cell counting kit-8 assay and colony formation assay

Cell counting kit-8 (CCK-8) and colony formation assays were conducted to assess the proliferation of OSA cells. For the CCK-8 assay, MG63 and 143B cells with si-control or si-RPS28 were seeded in 96-well plates in triplicate at a density of 3×10^3 cells/well. The cell viability was evaluated quantitatively at the indicated time points by adding 100 μL fresh culture medium with 10 % CCK-8 reagent (Dojindo Laboratories, Kumamoto, Japan) to each well after removing the old medium, followed by incubation at 37 °C for 1 h and detecting the optical density at 450 nm by using a microplate reader (BIOTEK, Vermont, USA).

For the colony formation assay, MG63 and 143B cells with si-control or si-RPS28 were seeded in 6 cm dishes in triplicate at a density of 1×10^3 cells/dish, then cultured with the medium replaced every three days. After one week, colonies were fixed with 4 % paraformaldehyde, stained with 1 % crystal violet, washed with phosphate-buffered saline (PBS) solutions, and photographed. The number of clones with more than 50 cells was counted.

2.9. Wound healing and matrigel invasion assays

For the wound healing assay, MG63 and 143B cells with si-control or si-RPS28 were seeded in 6-well plates in triplicate following nutrient deprivation for 12 h prior to seeding. Cells were scratched with a 200 μL sterile pipette tip to make a gap when the cell density reached approximately 90 %, which were further cultured in serum-free medium for 24 h. The sizes of gaps were observed and photographed at 0 and 24 h by CKX41 inverted microscopy (Olympus, Tokyo, Japan) and analyzed with Fiji Image J Software.

Matrigel invasion assays were carried out with Corning® BioCoat™ Matrigel Invasion Chambers (#354480)(Corning, NY, USA). After nutrient deprivation for 12 h, 5×10^4 cells with 100 μL serum-free DMEM were seeded into the upper chamber, whose lower chamber was added 600 μL DMEM with 10 % FBS. After incubation for 72 h, cells in the bottom chamber were stained, imaged, and counted by randomly selecting 3 fields of view to observe cells under a 100× microscope.

2.10. RNA sequencing, differentially expressed genes (DEGs) and enrichment analysis

After si-RPS28 and si-control treatments, total RNA of each group was extracted by TRIzol (Invitrogen) reagent. Then, RNA-sequencing was performed and its data was analysis (Niuke, Shanghai). The R software package limma was used for differential analysis to obtain the differential genes between the osteosarcoma group and the normal control group. Genes with a fold-change (FC) > 1.5 or < 0.67 (corresponds to $|\log2FC| \geq 0.585$) and p-value < 0.05 were considered significant DEGs. Kyoto Encyclopedia of Genes and Genomes (KEGG) terms were identified with a strict cutoff of $p < 0.01$ and a false discovery rate (FDR) of < 0.05.

2.11. In situ osteosarcoma mice model of tibia

All animal procedures performed in this study were conducted following the guidelines of the Animal Ethics Committee and approved by the relevant authorities (ethics approval number: DWSY2021-0158). Balb/c nude mice were obtained from GemPharmatech Co., Ltd (Nanjing, China). Stable expression of sh-RPS28 was achieved by introducing Virus-freeTM carriers (Cas9x, Suzhou, China) into 143B cells using the Neon™ electroporator (Invitrogen, USA). The mice were randomly divided into two groups, with each group consisting of five mice ($n = 5$). A total of 5×10^6 modified 143B cells were then injected into the medullary cavity of the tibia in 6-week-old male mice. On the 25th and 39th days after injection, an animal MRI was performed to measure the tumor size. Tumor volumes were calculated using the following formula: the sum of tumor areas multiplied by the slice thickness, calculated using RadiAnt DICOM Viewer (USA). At the end of the experiment, the mice were euthanized by decapitation under general anesthesia. The left legs containing the tumors were weighed using an electronic scale. Histological analysis including H&E staining and immunohistochemistry was performed as described earlier.

2.12. Statistical and other computational analyses

Unless stated otherwise, statistical analyses were conducted based on the R language (version 4.2.3) (https://cran.r-project.org/) and GraphPad Prism Version 9.0 software. The hazard ratios (HRs) and the 95 % confidence intervals (CIs) were determined using univariate as well as multivariate Cox regression models. All experiments were performed at least three times independently, and results are expressed as means ± standard deviation (SD). The student's *t*-test was used to analyze the differences between the two groups. The differences were considered significant if p-value < 0.05.

3. Results

3.1. Screen and selection of essential genes, and their characteristics

Initially, a gene screening for essential genes in osteosarcoma growth

was conducted using DepMap, a CRISPR-based database for genome-wide loss-of-function screening. This analysis utilized available gene effect scores (Chronos) on 13 OSA cell lines. Lower Chronos scores indicate a higher likelihood of gene essentiality in the specified cell lines. Negative scores indicate the genes' essential role in the proliferation of OSA cells (Fig. 1a). Subsequently, an enrichment analysis of these essential genes was performed to identify critical signal pathways. The results of GSEA revealed significant enrichment in the ribosome, proteasome, and spliceosome pathways which are in the top three according to normalized enrichment score (NES) (Fig. 1b). A set of 195 genes were identified after intersecting the essential genes with ribosome-related genes (Fig. 1c). To further identify hub essential ribosome-related genes, univariate COX regression analysis was then carried out using two data sets: TARGET-OSA and GSE21257-OSA. With the exception of *Lsg1* and *Ercc2*, the remaining ribosome-related genes were classified as risk genes (Fig. 1d). After intersecting the risk genes from both data sets, three potential ribosomal protein (RP) genes (*Rps28*, *Rps7*, *Rps25*) were initially validated (Fig. 1e).

3.2. Clinical validation and significance of Rps28 expression in OSA samples

Kaplan-Meier survival analysis of *Rps28* expression levels in two OSA data sets was conducted. High expression of *Rps28* was found to correlate with shorter overall survival (OS) (log-rank, p value = 0.0026 in TARGET-OSA; log-rank, p value = 0.014 in GSE21257) and progression-free survival (PFS) (log-rank, p value = 0.018 in TARGET-OSA; log-rank, p value = 0.012 in GSE21257), suggesting it may serve as a significant poor prognostic factor (Fig. 2a). Moreover, the expression of *Rps28* was higher in OSA cell lines compared with osteoblasts and mesenchymal stem cells (Fig. 2b). Immunofluorescence staining of U2OS cells from Human Protein Atlas (HPA) revealed cytoplasmic localization of eS28 proteins, with minimal staining in the nucleus (Fig. 2c). In conclusion, *Rps28*, an essential gene, may act as a poor prognostic factor and a potentially exploitable target in OSA.

To further validate the clinical significance of eS28 in OSA, immunohistochemical staining of eS28 protein was performed in tumor samples from five patients with tumor necrosis rates below 90 % (Table 1). The results revealed intensive expression of eS28 protein in OSA tissues, while its expression was rare in *para*-tumor soft tissue. Consistent with the results from HPA, eS28 proteins mainly overexpress

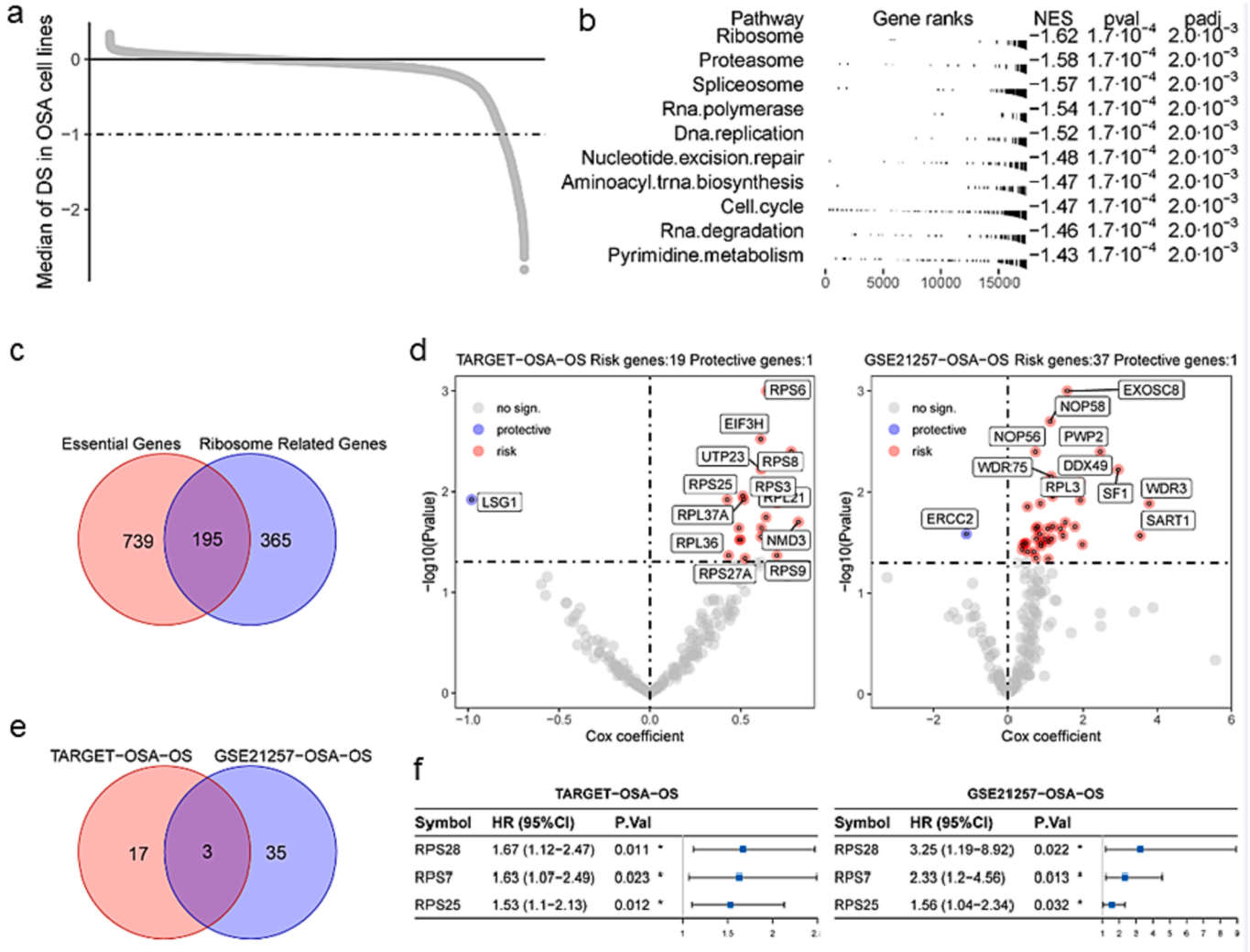

Fig. 1. Screen and selection of essential genes (a) Gene effect scores (Chronos): Scores representing the impact of genes on survival, calculated using the Chronos algorithm. (b) Enrichment analysis of essential genes in 13 OSA cell lines using GSEA. (c) The number of genes that overlap between the essential gene set and genes involved in ribosome biogenesis or function. (d) Univariate Cox analysis: Survival analysis conducted on TARGET-OSA and GSE21257-OSA datasets. (e) The intersection of risk genes (hazard radio > 1) between TARGET-OSA and GSE21257-OSA datasets. (f) Multivariate Cox analysis: Survival analysis evaluating the impact of three candidate genes on TARGET-OSA and GSE21257-OSA datasets.

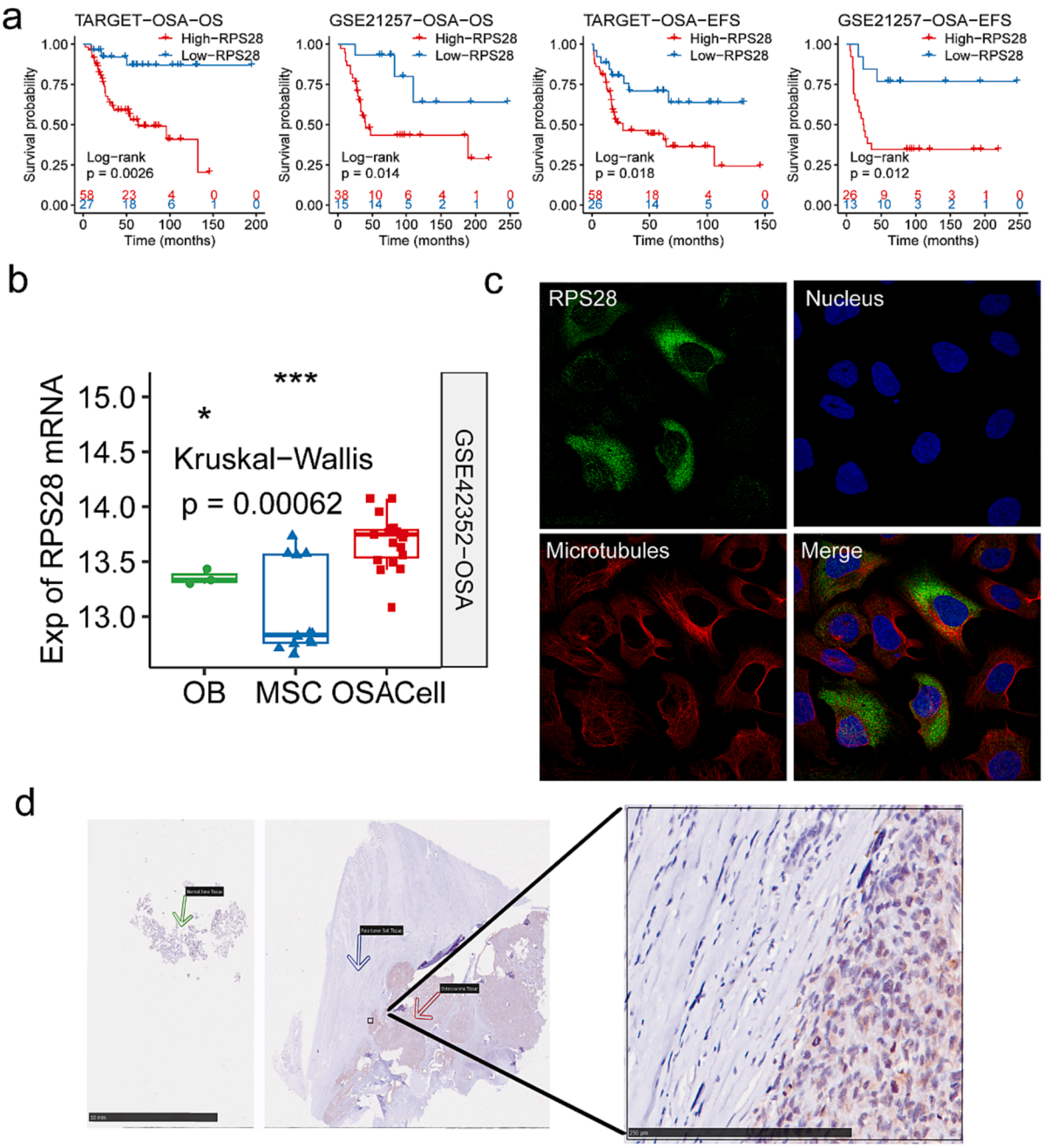

Fig. 2. High expression of *Rps28* is associated with poor prognosis in osteosarcoma. (a) The overall survival in the low/high *Rps28* expression group was analyzed in the TARGET-OSA data set. The disease-free survival in the low/high *Rps28* expression group was analyzed in the GSE21257-OSA data set. The P-value was calculated using Log-rank test. (b) Expression of *Rps28* between OSA cells, osteoblasts, and mesenchymal stem cells. (c) Immunofluorescence staining of eS28 on U2OS from HPA. Green fluorescence marks RPS proteins, blue fluorescence marks the nucleus, and red fluorescence marks microtubules. (d) Immunohistochemistry on samples of clinical patients after neoadjuvant chemotherapy. The blue arrow represents *para*-cancerous tissue and the red arrow represents cancerous tissue. One-way ANOVA with the Bonferroni *t*-test for multiple comparisons. $*p < 0.05$, $***p < 0.001$. (For interpretation of the references to colour in this figure legend, the reader is referred to the web version of this article.)

in cytoplasm. Notably, all samples with poor response presented positive staining (Fig. 2d, S1). A previous report suggested that decreased concentrations of eS28 protein had an impact on the viability of Hela cells [12]. Based on this observation, we speculated that eS28 might be directly involved in OSA development. This hypothesis was further investigated through in *vitro* and in *vivo* experiments.

3.3. Knockdown of eS28 reduced proliferation rate and lung metastasis in osteosarcoma in vitro and in vivo

In multiple OSA cell lines, MG63 and 143B exhibited higher expression of *RPS28* mRNA measured by qPCR and WB (Fig. 3a, S2a, S2b). Therefore, these two cell lines were selected for further RNA interference experiments, and si-RPS28-3 showed the most effective interference in reducing *Rps28* expression (Fig. 3b, S2a, S2c). CCK-8 assays were performed to assess the effect of eS28 knockdown on cell proliferation. The results showed that the knockdown of eS28

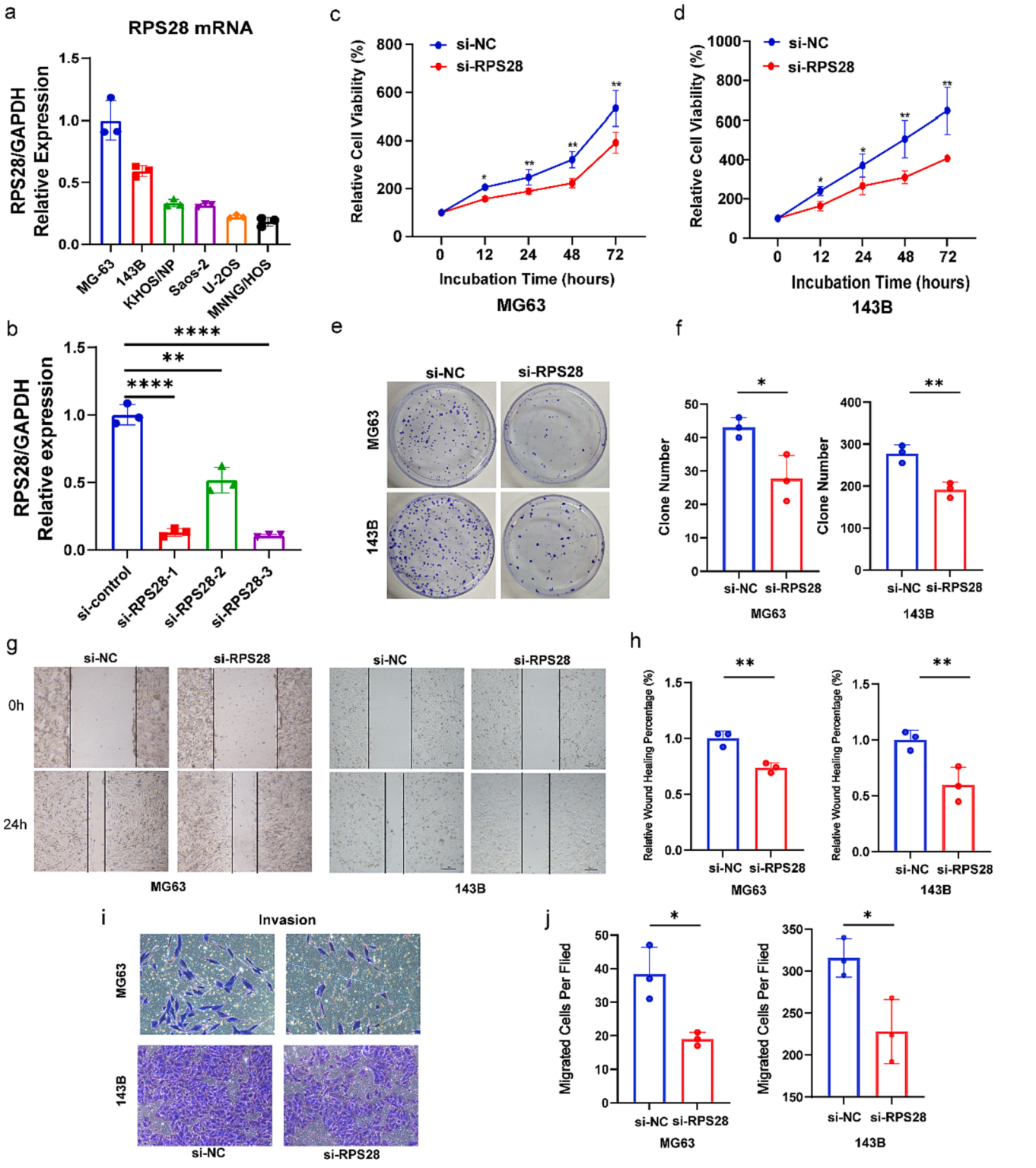

Fig. 3. The role of knockdown of eS28 on MG63 and 143B osteosarcoma cells. (a) Relative mRNA expression of *Rps28* in human OSA cell lines. (b) Relative mRNA expression of *Rps28* in MG-63 cell lines after transfection of si-control, si-RPS28-1, si-RPS28-2, si-RPS28-3. One-way ANOVA with the Bonferroni *t*-test for multiple comparisons. ns, no significance, $^{**}p < 0.01$, $^{****}p < 0.0001$. (c-d) Cell Counting Kit-8 Assay was performed to determine the rate of cell proliferation. (e-f) Clone formation assays on MG63 and 143B cells with/without knockdown of eS28. (g-h) Wound Healing assays were performed to determine the ability of cell migration. (i-j) Matrigel Invasion Assays were performed to determine the ability of cell invasion. Student's *t*-test, $^{*}P < 0.05$, $^{**}P < 0.01$.

significantly inhibited the proliferation rate of MG63 and 143B cells (Fig. 3c-3d). Colony formation assays were carried out to assess the cell population dependence besides cell proliferation. ES28 knockdown suppressed colony formation, indicating that eS28 knockdown not only inhibited the viability of cells, but also weakened cloning capabilities of MG-63 and U2OS cells. Notably, in 143B cells with eS28 knockdown, the inhibition of cell proliferation was greater than 50 % (Fig. 3e-3f). Furthermore, considering the association of eS28 with OSA metastasis,

wound healing assay and matrigel invasion assay were conducted. These assays demonstrated that the knockdown of eS28 moderately inhibited cell migration in MG63 and 143B cells, indicating the potential role of RPS28 in OSA metastasis (Fig. 4g-4j). However, in cell apoptotic experiments, no significant differences were observed between cells with eS28 knockdown and control cells (Figs. S3–S5). To further identify the role of eS28 downregulation in cell cycle, the cell cycle distribution was detected by flow cytometry. Cell cycle analysis showed that MG63 and 143B treated with siRNA-RPS28 had a slight increase of cells in the G0/G1 phase compared with control groups, representing that down-regulating eS28 might be responsible for influences in the osteosarcoma cell cycle (Fig. S6). These results suggested that eS28 may play a significant role in regulating OSA cell proliferation cell cycle, and metastasis, while its effect on apoptosis remains inconclusive.

In vivo experiments, balb/c nude mice models were conducted to further investigate the function of the eS28. 143B cells with stable expression of sh-RPS28 were tested by WB (Fig. S7a-S7b). The models were established via injection of sh-RPS28 and sh-control 143B cells.

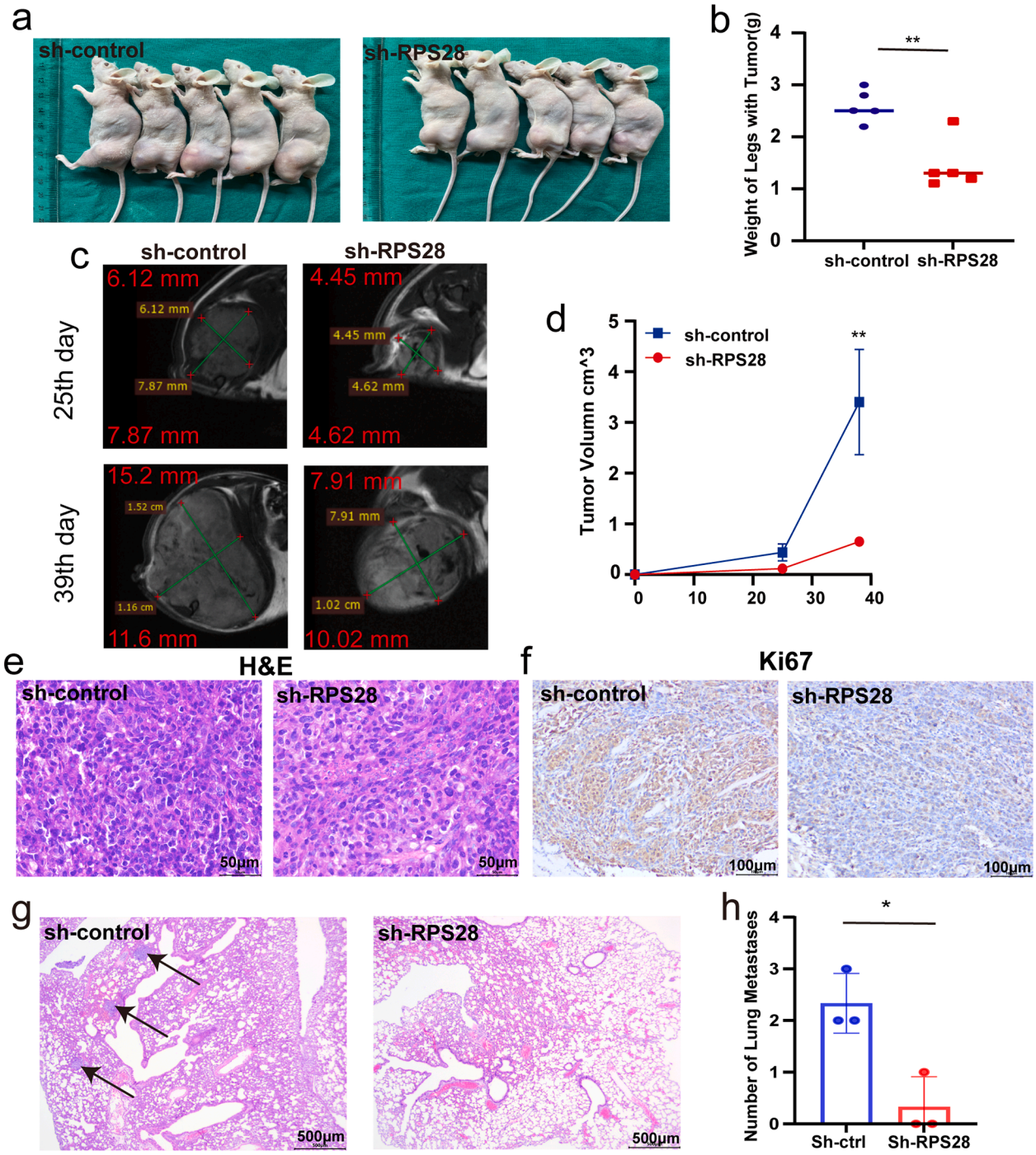

Fig. 4. Knockdown of eS28 delayed progression of tumor *in vivo* (a) The mice were sacrificed for tumor harvesting and tumor image. (b) Tumor weight of legs with tumor was measured in sh-control and sh-RPS28 group. (c) The accurate measure of tumor size by animal MRI on days 25th and 39th. (d) The tumor growth curves were plotted in sh-control group and sh-RPS28 groups. Statistical significance was calculated via two-way ANOVA with Bonferroni's test, $^{**}P < 0.01$. (e) H&E staining for tumor. (f) Ki67 staining for tumor. (g) H&E staining for lung. Arrows indicated lung metastatic sites. (h) The number of lung metastases in the sh-control and sh-RPS28 groups. Student's *t*-test, $^{*}P < 0.05$.

The nude mice with eS28 knockdown exhibited smaller tumor volumes compared with the control group, and the weight of legs with tumor could conform to it (Fig. 4a-4b). To accurately measure the tumor volume, an animal MRI designed for mice was performed on the 25th and 39th days of the study. Results showed larger tumor masses in the control group (Fig. 4c-4d). H&E and Ki67 staining, used to assess osteosarcoma proliferation at the pathological level, indicated a weaker proliferative capacity in the sh-RPS28 group (Fig. 4e-4f). After random selection of three lung examples from two groups, the sh-RPS28 group showed almost no metastasis, whereas several obvious metastatic foci were observed in the control group (Fig. 4g-4h). Overall, the knockdown of eS28 inhibited the proliferation and invasion of osteosarcoma but did not affect apoptosis of osteosarcoma in both in *vitro* and in *vivo* experiments.

3.4. Silencing Rps28 affected the MAPK signaling pathway

In order to understand the functional implications of eS28 in OSA, transcriptome sequencing was performed on 143B cells with and without sh-RPS28. The knockdown of eS28 resulted in approximately 50 % reduction in RPS28 mRNA expression compared with control groups. Differential gene analysis revealed that 803 genes were upregulated, and 852 genes were downregulated when RPS28 was knocked down. Volcano plots and heatmaps were generated to visualize the differential gene expression (Fig. 5a, S8). KEGG pathway analysis showed that differentially expressed genes were significantly enriched in gene sets related to the tumor necrosis factor (TNF), interleukin 17 (IL-17), and MAPK signaling pathways (Fig. 5b). GSEA analysis, which considers all differentially expressed genes without neglecting potentially important genes, also highlighted the enrichment of the MAPK signaling pathway (Fig. 5c). Intriguingly, the ribosome pathway was also enriched (Fig. 5d). To validate the involvement of the MAPK

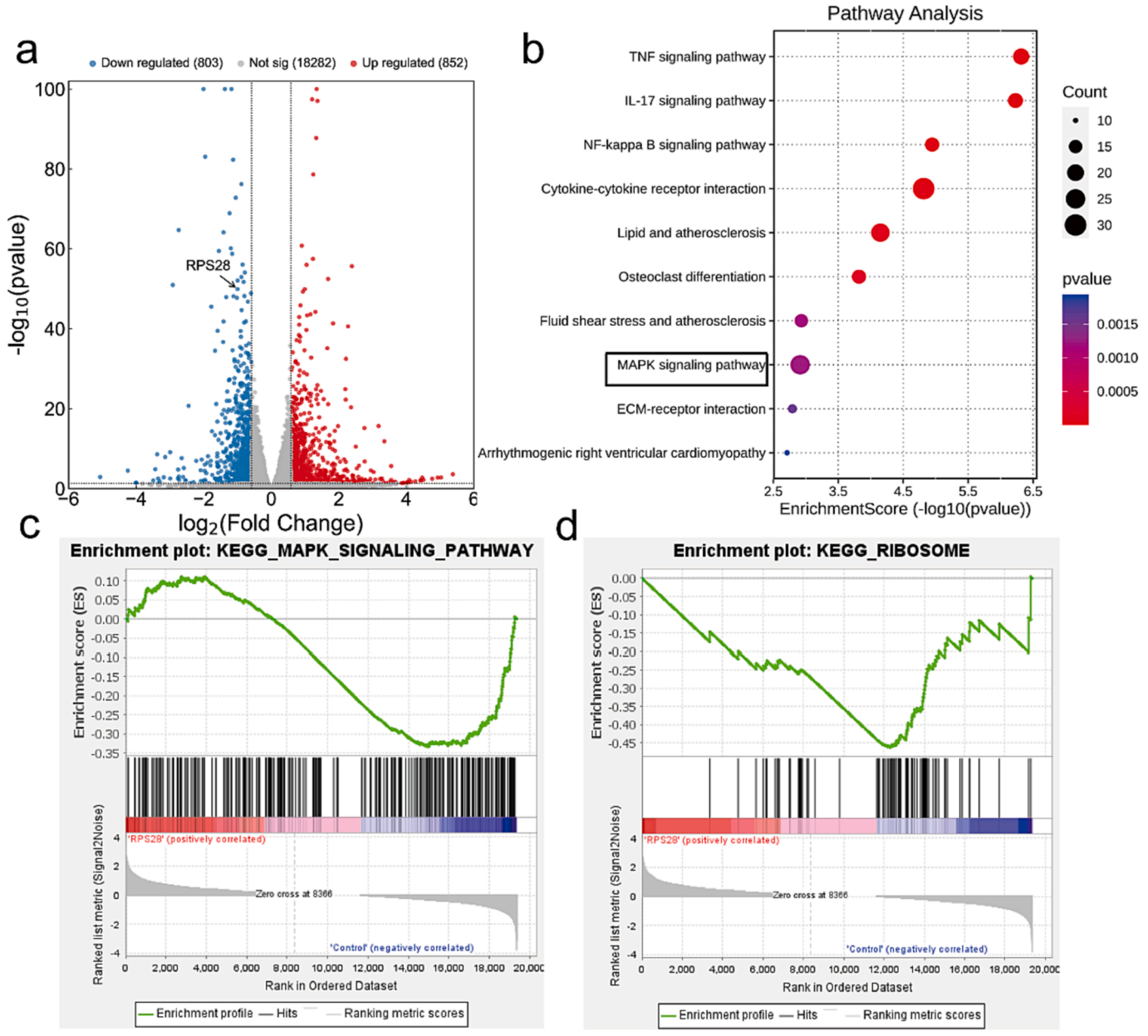

Fig. 5. Differential and Enrichment Analysis for silencing *Rps28* (a-b) (c) Volcano plot (logFC > 1.5, p < 0.05). (d) The top 10 main signal pathways were presented by KEGG enrichment analysis for eS28 knockdown. (e-f) The MAPK and ribosome signal pathways were mainly enriched by GSEA enrichment analysis.

signaling pathway, indicators related to this pathway were examined in MG63 and 143B cells treated with si-RPS28. Silencing *Rps28* resulted in the suppression of ERK1/2 phosphorylation, indicating reduced pathway activation (Fig. 6a-6b). Moreover, the expression of c-myc, which is stabilized by phosphorylated p-ERK1/2, was downregulated as well (Fig. 6a-6b). These findings suggested that eS28 knockdown affected the MAPK signaling pathway in OS cells.

4. Discussion

The mutated oncogenes and tumor suppressor genes responsible for cancer development can impart distinct properties to cancer cells, creating dependencies on specific genes that differ from normal cells [13,14]. These genes have the potential to be promising candidates for developing molecularly targeted drugs [15]. By systematically identifying and characterizing these genes, we can uncover promising candidates for targeted cancer treatments. CRISPR-Cas9 library genome screening is capable of accurate negative selections [16–18]. This screening can reveal what genes are essential for survival under specific conditions, such as cell type and oncogene status. For example, PCMT1 was regarded as a critical driver of ovarian cancer metastasis through a CRISPR/Cas9 library screen [19]. In the present research, we first identified essential genes based on the DepMap database, a large-scale CRISPR-Cas9 and RNAi database. Gene dependencies in 13 kinds of osteosarcoma cell lines are recorded in the database [20]. GSEA analysis revealed that these essential genes were mainly enriched in the ribosome pathway. By univariate COX regression and multivariate COX regression analyses, *Rps28* was finally found as an independent and significant risk factor. Kaplan-Meier survival analyses were validated further. Due to the high expression of high by comparison between OSA tissues and normal tissues at the mRNA level and protein level, there is the possibility of eS28 as a potential drug target.

Ribosomes play a crucial role in protein synthesis by translating mRNA into functional proteins. Abnormal ribosome biogenesis, often triggered by oncogenes or the loss of tumor suppressor genes, is closely associated with the development and progression of cancer [21–23]. The hyperactivation of ribosome biogenesis has been identified as a critical factor in cancer initiation and progression. *Rps28* gene, located at 19p13.2, encodes a ribosomal protein, eS28, that is a component of the small 40S subunit. *Rps28* expression is associated with multiple tumor progression and prognosis [24,25]. Hak Kyun Kim et al found inhibition of LeuCAG3′tsRNA reduces *Rps28* mRNA translation, resulting in reduced 18S rRNA processing and lower numbers of 40S ribosomal subunits. A report showed that eS28 controls MHC class I peptide generation and influences $CD8^+$ T cell cancer immunosurveillance in melanoma [26]. Additionally, in *vitro* experiments showed that eS28 knockdown impaired the proliferation, migration, and invasion of MG63 cell lines. In addition, a decrease in translation of *Rps28* mRNA blocks pre-18S ribosomal RNA processing, resulting in a reduction in the number of 40S ribosomal subunits, and ultimately induces apoptosis [12]. However, we failed to observe the significant apoptosis in OSA with eS28 knockdown. This difference may be explained by the origin of different tumor cells.

RPs have been neglected since a long time ago, mainly because many

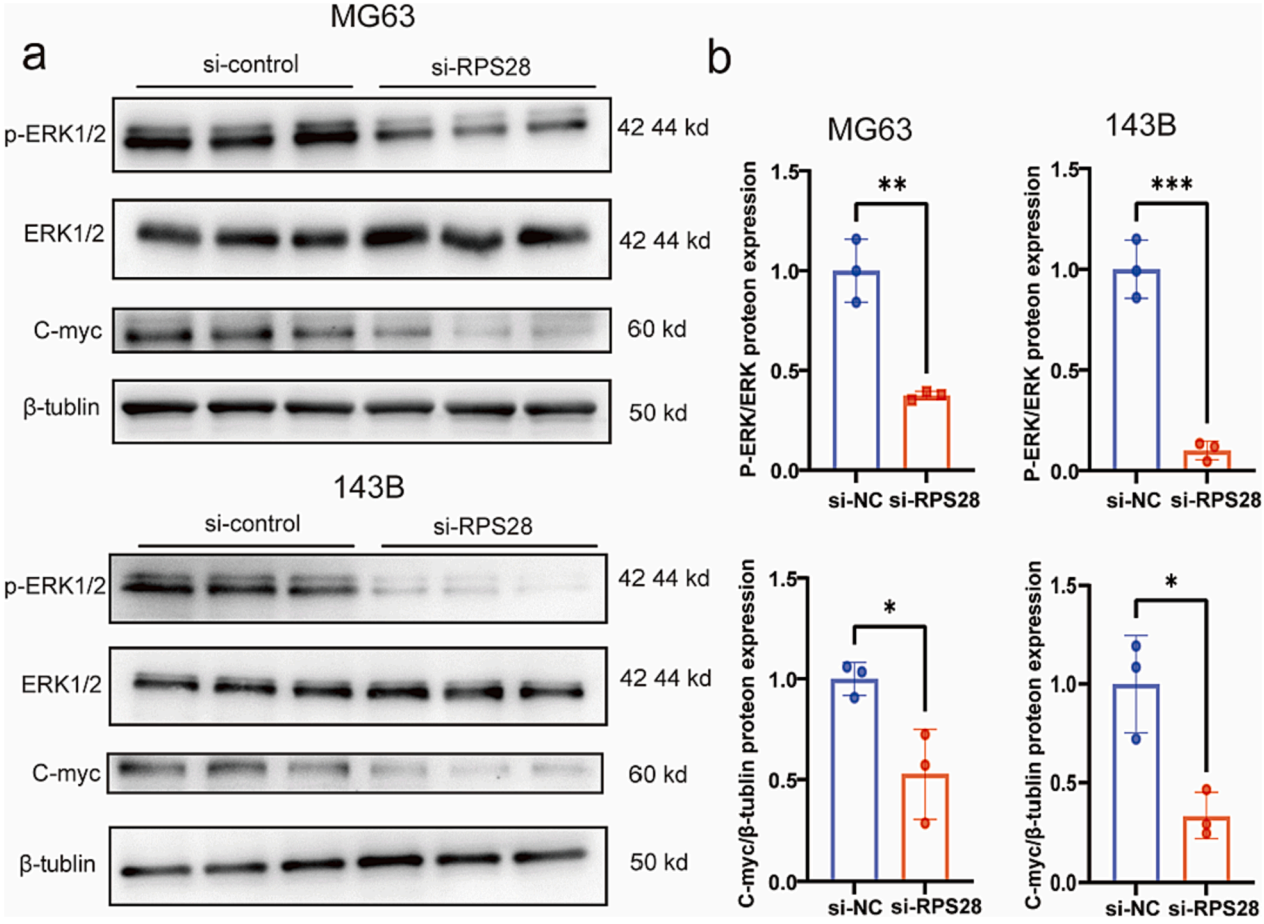

Fig. 6. Knockdown of eS28 decreased ERK1/2 phosphorylation, leading to down-regulation of c-myc expression. (a) Protein expression changes of phospho-ERK were analyzed by western blot analysis assays using 143B and MG63 cells with/without eS28 knockdown. The c-myc expression, the downstream of ERK1/2 MAPK signal pathway, was also measured by western blot analysis. (b) Statistical analysis on protein expression changes of phospho-ERK, ERK and c-myc. Student's *t*-test, $^*P < 0.05$, $^{**}P < 0.01$, $^{***}P < 0.001$.

people think that they are merely housekeeping genes involved in protein synthesis. Currently, researchers believe the extra-ribosomal function of RPs can regulate diverse cellular processes including cell cycle, DNA repair, maintenance of genome integrity, cellular proliferation, apoptosis, autophagy, cell migration, and invasion [27,28]. Ribosomal protein S6 (RPS26) promoted sphere-forming ability and stem cell marker expression in GB cells [29,30]. In our study, KEGG and GSEA analysis predicted the MAPK signal pathway as a target of eS28 acting on OSA, and the results of the western blot showed that the knockdown of eS28 weakened the phosphorylation of ERK1/2. In addition, the mechanism by which loss of eS28 impact osteosarcoma cell properties could be partly explained by the ribosomal dysregulation of the protein.

Some limitations still existed in our study. Firstly, the down-regulation of eS28 showed an inhibited effect rather than toxicity on OSA cells. Combination with chemotherapy may be a strategy in the future. Secondly, the detailed mechanisms underlying how eS28 exerted its effects mentioned above require further exploration. At last, more clear evidence for eS28 as a potential therapeutic target in osteosarcoma will be needed.

5. Conclusion

Through analysis of the DepMap database, *Rps28* gene has been identified as essential for the survival of osteosarcoma cells. Besides its conventional role in protein synthesis, eS28 has been found to function as an oncogene in osteosarcoma and is associated with the MAPK signaling pathway. This study suggested that eS28 may play a crucial role in the proliferation and progression of osteosarcoma by impacting the MAPK signaling pathway. These findings provide valuable insights into the underlying mechanisms of osteosarcoma pathogenesis and offer potential avenues for therapeutic approaches.

CRediT authorship contribution statement

Chao Liang: . **Juan Zhou:** Methodology. **Yongjie Wang:** . **Yin Sun:** Resources. **Jin Zhou:** Resources. **Lan Shao:** Resources. **Zhichang Zhang:** Data curation, Formal analysis. **Wangjun Yan:** Investigation, Project administration, Supervision. **Zhiyan Liu:** Methodology, Visualization. **Yang Dong:** Project administration, Supervision.

Declaration of competing interest

The authors declare that they have no known competing financial interests or personal relationships that could have appeared to influence the work reported in this paper.

Acknowledgments

We thank Lin Zeng for his technical advice.

Funding

This research was supported by grants from the National Natural Science Foundation of China (82072962)(82272869).

Appendix A. Supplementary data

Supplementary data to this article can be found online at https://doi.org/10.1016/j.jbo.2023.100517.

References

[1] J. Ritter, S.S. Bielack, Osteosarcoma, Ann. Oncol. 21 Suppl 7 (2010) vii320-5.
[2] P.S. Meltzer, L.J. Helman, New Horizons in the Treatment of Osteosarcoma, N. Engl. J. Med. 385 (22) (2021) 2066–2076.
[3] A. Smrke, et al., Future Directions in the Treatment of Osteosarcoma, Cells 10 (1) (2021).
[4] Z. Hu, et al., Current Status and Prospects of Targeted Therapy for Osteosarcoma, Cells 11 (21) (2022).
[5] M. Chen, et al., CRISPR-Cas9 for cancer therapy: Opportunities and challenges, Cancer Lett. 447 (2019) 48–55.
[6] X. Feng, et al., Genome-wide CRISPR screens using isogenic cells reveal vulnerabilities conferred by loss of tumor suppressors, Sci. Adv. 8(19) (2022) eabm6638.
[7] A. Tsherniak, et al., Defining a Cancer Dependency Map, Cell 170 (3) (2017) 564–576.e16.
[8] M. Kurata, et al., CRISPR/Cas9 library screening for drug target discovery, J. Hum. Genet. 63 (2) (2018) 179–186.
[9] Y.T. Chan, et al., CRISPR-Cas9 library screening approach for anti-cancer drug discovery: overview and perspectives, Theranostics 12 (7) (2022) 3329–3344.
[10] J.M. Dempster, et al., Chronos: a cell population dynamics model of CRISPR experiments that improves inference of gene fitness effects, Genome Biol. 22 (1) (2021) 343.
[11] R.M. Meyers, et al., Computational correction of copy number effect improves specificity of CRISPR-Cas9 essentiality screens in cancer cells, Nat. Genet. 49 (12) (2017) 1779–1784.
[12] H.K. Kim, et al., A transfer-RNA-derived small RNA regulates ribosome biogenesis, Nature 552 (7683) (2017) 57–62.
[13] H.J. Uckelmann, et al., Mutant NPM1 Directly Regulates Oncogenic Transcription in Acute Myeloid Leukemia, Cancer Discov. 13 (3) (2023) 746–765.
[14] D. Zingg, et al., Truncated FGFR2 is a clinically actionable oncogene in multiple cancers, Nature 608 (7923) (2022) 609–617.
[15] T. Hart, et al., High-Resolution CRISPR Screens Reveal Fitness Genes and Genotype-Specific Cancer Liabilities, Cell 163 (6) (2015) 1515–1526.
[16] S.A. Hosseini, et al., CRISPR/Cas9 as precision and high-throughput genetic engineering tools in gastrointestinal cancer research and therapy, Int. J. Biol. Macromol. 223 (Pt A) (2022) 732–754.
[17] Z. Zeng, et al., Identifying novel therapeutic targets in gastric cancer using genome-wide CRISPR-Cas9 screening, Oncogene 41 (14) (2022) 2069–2078.
[18] K. Balon, et al., Targeting Cancer with CRISPR/Cas9-Based Therapy, Int. J. Mol. Sci. 23 (1) (2022).
[19] J. Zhang, et al., Genome-wide CRISPR/Cas9 library screen identifies PCMT1 as a critical driver of ovarian cancer metastasis, J. Exp. Clin. Cancer Res. 41 (1) (2022) 24.
[20] W. Chen, et al., Identification of LARS as an essential gene for osteosarcoma proliferation through large-Scale CRISPR-Cas9 screening database and experimental verification, J. Transl. Med. 20 (1) (2022) 355.
[21] J. Kang, et al., Ribosomal proteins and human diseases: molecular mechanisms and targeted therapy, Signal Transduct. Target. Ther. 6 (1) (2021) 323.
[22] A.R. Elhamamsy, et al., Ribosome Biogenesis: A Central Player in Cancer Metastasis and Therapeutic Resistance, Cancer Res. 82 (13) (2022) 2344–2353.
[23] J. Pelletier, G. Thomas, S. Volarević, Ribosome biogenesis in cancer: new players and therapeutic avenues, Nat. Rev. Cancer 18 (1) (2018) 51–63.
[24] C. Yau, et al., A multigene predictor of metastatic outcome in early stage hormone receptor-negative and triple-negative breast cancer, Breast Cancer Res. 12 (5) (2010) R85.
[25] Z. Huang, et al., Identification and validation of seven RNA binding protein genes as a prognostic signature in oral cavity squamous cell carcinoma, Bioengineered 12 (1) (2021) 7248–7262.
[26] J. Wei, et al., Ribosomal Proteins Regulate MHC Class I Peptide Generation for Immunosurveillance, Mol. Cell 73 (6) (2019) 1162–1173.e5.
[27] W. El Khoury, Z. Nasr, Deregulation of ribosomal proteins in human cancers, Biosci. Rep. 41 (12) (2021).
[28] X. Xu, X. Xiong, Y. Sun, The role of ribosomal proteins in the regulation of cell proliferation, tumorigenesis, and genomic integrity, Sci. China Life Sci. 59 (7) (2016) 656–672.
[29] T. Hide, et al., Ribosomal proteins induce stem cell-like characteristics in glioma cells as an "extra-ribosomal function", Brain Tumor Pathol. 39 (2) (2022) 51–56.
[30] Y.W. Yi, et al., Ribosomal Protein S6: A Potential Therapeutic Target against Cancer? Int. J. Mol. Sci. 23 (1) (2021).